

# A quantum model for rf-SQUIDs based metamaterials enabling 3WM and 4WM Travelling Wave Parametric Amplification

Angelo Greco and Luca Fasolo

*INRiM, Istituto Nazionale di Ricerca Metrologica,  
Strada delle Cacce 91, 10135 Torino, Italy and  
Department of Electronics and Telecommunications,  
Politecnico di Torino, Corso Castelfidardo 39, 10129 Torino, Italy*

Alice Meda, Luca Callegaro, and Emanuele Enrico\*

*INRiM, Istituto Nazionale di Ricerca Metrologica, Strada delle Cacce 91, 10135 Torino, Italy*

(Dated: March 28, 2025)

A quantum model for Josephson-based metamaterials working in the Three-Wave Mixing (3WM) and Four-Wave Mixing (4WM) regimes at the single photon level is presented. The transmission line taken into account, namely Traveling Wave Josephson Parametric Amplifier (TWJPA), is a bipole composed by a chain of rf-SQUIDs which can be biased by a DC current or a magnetic field in order to activate the 3WM or 4WM nonlinearities. The model exploits a Hamiltonian approach to analytically work out the time evolution both in the Heisenberg and interaction pictures. The former returns the analytic form of the gain of the amplifier, while the latter allows to recover the probability distributions vs. time of the photonic populations, for multimodal Fock and coherent input states. The dependence of the metamaterial's nonlinearities is presented in terms of circuit parameters in a lumped model framework while evaluating the experimental conditions effects on the model validity.

## I. INTRODUCTION

Superconducting amplifiers are nowadays widely used for the detection of single photons in several ranges of the electromagnetic spectrum. From microwaves to X-rays these devices have shown unrivalled performances for what concerns quantum efficiency, resolving power and added noise, compared to their solid state counterparts [1–6]. The peculiar characteristics of superconducting materials allow to engineer highly performing resonators and cavities, characterised by quality factor of the order of  $\approx 10^{10}$  [7–10]. Indeed, resonator-based superconducting amplifiers show a quite high gain, in the range of 20 dB [9], however, they are subjected to a limited bandwidth, fact that makes them unsuitable for the multiplexing required in complex systems.

Traveling Waves Josephson Parametric Amplifiers (TWJPAs) and Kinetic Inductance Traveling Wave Amplifiers (KITs) promise to be appropriate devices for this aim in the microwave regime, showing in principle valuable multiplexing capabilities due to their wide bandwidth [11]. Indeed, it has been shown how the Four-Wave Mixing (4WM) induced in all the Kerr-like media allows amplifying very tiny signals over a several GHz bandwidth with a minimum amount of added noise [11–14]. Nevertheless, recent papers show that, enabling the Three-Wave Mixing (3WM) interaction, through the introduction of a quadratic non-linearity

in the medium, could provide several benefits and experimental simplifications for what concerns feasibility and integration capabilities. In particular, a three-wave mixer generally requires a lower input pump power, an easier output filtering and shows a higher dynamic range [15–17]. These distinctive characteristics make TWJPAs working in 3WM excellent candidates for the readout of quantum limited detectors (e.g., rf-SETs, rf-SQUIDs), by preserving the quantum properties of their outputs [18–20]. Moreover, a three-wave mixer can be a promising candidate for the generation of heralded photons pairs, since it naturally enables Parametric Down Conversion (PDC) [21].

In this framework we develop a quantum model, based on previous theoretical works [22, 23], for a recently proposed TWJPA concept [16] covering both the 3WM and 4WM regimes. Previous classical descriptions in terms of electromagnetic waves [16, 17] were limited to the high power range, completely neglecting any description of the light-matter interaction at the single photon level. Our theory exploits circuit-QED techniques to model a TWJPA made up of a chain of rf-SQUIDs capacitively shunted to ground. The proposed layout can be biased by a DC current or an externally applied magnetic field in order to activate 3WM or 4WM of the microwave traveling modes. The quantum description allows to analytically treat important figures of merit of the amplifier like gain, squeezing and time evolution of arbitrary quantum states at the single photon level. The main results of the paper are reported in Section II. In particular, Subsection II A reports the Hamiltonian in first quantization formalism, based on the

\* Corresponding author: e.enrico@inrim.it

circuit model of a nonlinear lossless transmission line. Then, Subsection II B is dedicated to develop the theory through the occupation number formalism, and a 3WM/4WM Hamiltonian is found. A selection of modes follows in Subsection II C, leading to model the 3WM/4WM quantum mechanical phenomena in the Heisenberg picture. Solving the dynamics of the system (i.e., Langevin equations) allows to analytically calculate the gain and squeezing capabilities of the amplifier. In Subsection II D the time evolution of Fock and coherent input states due to nonlinear interactions is analytically treated and on these basis various examples of photon statistics in the Fock space are calculated. The Discussion section III is focused on both the circuit parameter constraints bounded to physical and experimental requirements (Subsections III A) and on a clear outline of the limits of validity of the model (Subsection III C and III B).

## II. RESULTS

### A. rf-SQUIDs array embedded in a transmission line

The TWJPA recently proposed [16] and theoretically quantum mechanically treated in this paper can be modeled as an array of rf-SQUIDs embedded in a superconducting transmission line. In the following, the Hamiltonian of the system will be derived as a function of its circuit parameters. As represented in Figure 1, each elementary cell is composed by a superconducting loop containing a Josephson junction (with its associated capacitance  $C_J$  and inductance  $L_J$ ) and a geometrical inductance  $L_g$ . Furthermore, each loop is coupled to ground through a capacitor  $C_g$ . The system taken

into account is non-dissipative and, in sake of simplicity, all the elementary cells are considered equal. The length of the elementary cell along the  $z$ -direction (i.e., the propagating direction of the modes) is defined as  $a$ . In presence of an electromagnetic field, each of these cells stores a certain amount of energy that can be expressed as a function of the conjugate coordinates  $\hat{\Phi}$  and  $\hat{Q}$ , the generalized magnetic flux and charge at a certain node, respectively. The total amount of energy can be computed as the sum of the energy stored in each of its components (see Appendix A). Moreover, being the system under analysis a repetition of identical elementary units, the total energy stored in the whole medium can be expressed as the sum of the energy stored in each cell.

Under the assumption that the differences between the  $\hat{\Phi}$  (and  $\hat{Q}$ ) of a couple of consecutive nodes are small enough, these quantities can be considered as continuous functions of time and space (i.e.,  $\hat{\Phi}(z, t)$  and  $\hat{Q}(z, t)$ ). This consideration can also be applied to the definition of the total energy stored in the medium, leading to an expression in terms of an integral of a linear density Hamiltonian  $\hat{\mathcal{H}}$ :

$$\hat{\mathcal{H}} = \hat{\mathcal{H}}_{L_g} + \hat{\mathcal{H}}_{L_J} + \hat{\mathcal{H}}_{C_J} + \hat{\mathcal{H}}_{C_g} \quad (1)$$

where in the right-hand side of equation (1) one can recognize respectively the energy density associated to the geometrical inductance  $L_g$ , the Josephson inductance  $L_J$ , the Josephson capacitance  $C_J$  and the ground capacitance  $C_g$ .

Hence, the Hamiltonian of the whole system is the spatial integral across the  $z$ -axis and along a quantization length  $l_q = aN$  [24], of the linear Hamiltonian density in equation (1):

$$\hat{H} = \int_{l_q} \hat{\mathcal{H}} dz = \frac{1}{2a} \int_{l_q} dz \left[ 2I_c \varphi_0 \left( 1 - \cos \left( \frac{\Delta \hat{\Phi}}{\varphi_0} \right) \right) + \frac{1}{L_g} \Delta \hat{\Phi}^2 + C_J \left( \frac{\partial \Delta \hat{\Phi}}{\partial t} \right)^2 + \frac{\dot{Q}_{C_g}^2}{C_g} \right] \quad (2)$$

having identified  $\Delta \hat{\Phi}$  as the magnetic flux difference function across the cells,  $N$  as the number of unit cells composing the transmission line,  $I_c$  as the critical current of the Josephson junction,  $\varphi_0 = \hbar/2e$  as the reduced flux quantum, being  $\hbar$  the reduced Plank constant and  $e$  the elementary charge.

The presence of an external magnetic field or a DC current through the line induces a constant component in the flux difference across a cell. This means that  $\Delta \hat{\Phi}$  can be considered as the sum of two components, a con-

stant one  $\Delta \Phi_{DC}$  and a time-dependent one  $\delta \hat{\Phi}$

$$\Delta \hat{\Phi} = \Delta \Phi_{DC} + \delta \hat{\Phi} \quad (3)$$

### B. Second quantization framework

Here the Hamiltonian will be expressed in terms of ladder operators. In this view, the voltage drop on the ground capacitors  $C_g$  can be expressed using a mode decomposition assuming that sinusoidal waves are passing

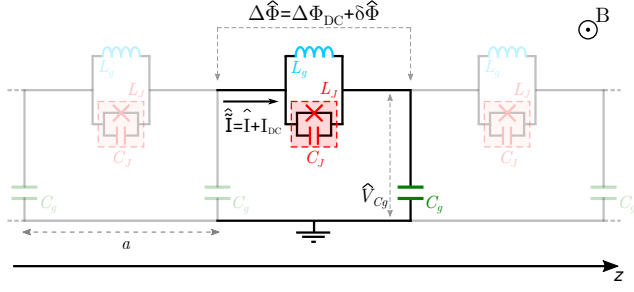


Figure 1. Electrical equivalent of a repetition of three elementary cells (periodicity  $a$ ) of the rf-SQUIDS based TWJPA. Each cell consists of a superconducting loop containing a geometrical inductance  $L_g$ , a Josephson junction, with an associated capacitance  $C_J$  and inductance  $L_J$ , and a ground capacitor  $C_g$ . The series can be biased both through an external DC magnetic field  $B$  and a flowing current  $I_{DC}$ .  $\Delta\hat{\Phi}$  is the magnetic flux difference across the nodes of a cell, while  $\hat{V}_{Cg}$  is the voltage drop across the ground capacitor.

through the line [25]

$$\hat{V}_{Cg}(z, t) = \sum_n \sqrt{\frac{\hbar\omega_n}{2C_g N}} \left( \hat{a}_n e^{i(k_n z - \omega_n t)} + \text{H.c.} \right) \quad (4)$$

where  $\omega_n$  and  $k_n$  are the angular frequency and wavenumber of the  $n$ -th mode while  $\hat{a}$  is its annihilation operator. Positive indexes denote progressive waves ( $k_n > 0$  and  $\omega_n > 0$ ), while negative indexes denote regressive waves ( $k_{-n} = -k_n < 0$  and  $\omega_{-n} = \omega_n$ ).

The link between the voltage drop and the current passing through a cell is straightforwardly found recalling the Telegrapher's equation, that exploits the inductance of the cell for the  $n$ -th mode  $\hat{L}_n$

$$\frac{\partial \hat{V}_n}{\partial z} = -\frac{\hat{L}_n}{a} \frac{\partial \hat{I}_n}{\partial t} \quad (5)$$

$\hat{L}_n$  can be calculated as the parallel between the effective inductance  $L_{\text{eff},n}$  (composed by the Josephson capacitance  $C_J$  and the geometrical inductance  $L_g$ , see Appendix B) and the nonlinear Josephson inductance  $\hat{L}_J$ . Exploiting the constitutive relation for a generic inductor it can be written that  $\Delta\hat{\Phi} = \hat{L}\hat{I}$ . Hence, using the flux-current relation of a Josephson junction,  $\hat{I}_J = I_c \sin(\Delta\hat{\Phi}/\varphi_0)$ , the nonlinear Josephson inductance  $\hat{L}_J$  can be simply expressed as

$$\hat{L}_J = \frac{\Delta\hat{\Phi}}{\hat{I}_J} = \frac{\varphi_0}{I_c} \frac{\Delta\hat{\Phi}/\varphi_0}{\sin(\Delta\hat{\Phi}/\varphi_0)} \equiv L_{J_0} \frac{\Delta\hat{\Phi}/\varphi_0}{\sin(\Delta\hat{\Phi}/\varphi_0)} \quad (6)$$

with  $L_{J_0} = \varphi_0/I_c$ . It follows that the cell inductance

$L_n$  can be written as

$$\hat{L}_n = \frac{\Lambda_n L_g}{1 + \Lambda_n \frac{L_g}{L_{J_0}} \frac{\sin(\Delta\hat{\Phi}/\varphi_0)}{(\Delta\hat{\Phi}/\varphi_0)}} \quad (7)$$

where the dispersion coefficient of the  $n$ -th node  $\Lambda_n = 1/(1 - \omega_n^2 L_g C_J)$  (Appendix B) has been defined. The time-dependent component of equation (3) can be found exploiting the mode decomposition for the AC current through the cell  $\hat{I}_n$  and the inductance  $\hat{L}_n$  for the corresponding mode as

$$\delta\hat{\Phi} = \sum_n \hat{L}_n \hat{I}_n \quad (8)$$

It follows that (see Appendix C)

$$\delta\hat{\Phi} = \sum_n \left[ \left( 1 + \Lambda_n \frac{L_g}{L_{J_0}} \frac{\sin\left(\frac{\Delta\Phi_{DC} + \delta\hat{\Phi}}{\varphi_0}\right)}{\frac{\Delta\Phi_{DC} + \delta\hat{\Phi}}{\varphi_0}} \right)^{-\frac{1}{2}} \delta\hat{\Phi}_n^{(0)} \right] \quad (9)$$

where the zero order AC flux component of the  $n$ -th mode  $\delta\hat{\Phi}_n^{(0)}$  has been defined. Equation (9) is a recursive relation for the nonlinear flux operator  $\delta\hat{\Phi}$ , which can be straightforwardly solved at zero order by the substitution  $\delta\hat{\Phi} \mapsto \delta\hat{\Phi}^{(0)}$  in the right-hand side.

In order to find an analytical solution one can perform the Taylor expansion of the square root of equation (9) and the Josephson energy into (3) for  $\delta\hat{\Phi}^{(0)} \ll \varphi_0$ . The maximum order of expansion was chosen in order to take into account scattering events involving at most 4 photons. This procedure provides a valid approximation for the nonlinear time-dependent flux operator  $\delta\hat{\Phi}$  that can be substituted into equation (2) in order to obtain the Hamiltonian of the system in terms of ladder operators.

$$\begin{aligned} \hat{H} = \hbar\chi_0 + \sum_n \hbar\chi_1^{(n)} \left( \hat{a}_n^\dagger \hat{a}_n + \frac{1}{2} \right) + \\ + \sum_{n,l,m} \hbar\chi_3^{(n,l,m)} \{ \hat{a} + \hat{a}^\dagger \}_{n,l,m} \delta_{\Delta\omega_{n,l,m}, 0} + \\ + \sum_{n,l,m,s} \hbar\chi_4^{(n,l,m,s)} \{ \hat{a} + \hat{a}^\dagger \}_{n,l,m,s} \delta_{\Delta\omega_{n,l,m,s}, 0} \end{aligned} \quad (10)$$

The subscripts of the braces in equation (10) stand for a multiplication of the form  $\{ \hat{a} + \hat{a}^\dagger \}_{n,l,\dots,k} = (\hat{a}_n + \hat{a}_n^\dagger)(\hat{a}_l + \hat{a}_l^\dagger) \dots (\hat{a}_k + \hat{a}_k^\dagger)$ . The  $\delta_{\Delta\omega,0}$  Kronecker functions have the role to select the only scattering events that fulfill the energy conservation between the three ( $\Delta\omega_{n,l,m} = 0$ ) or four ( $\Delta\omega_{n,l,m,s} = 0$ ) modes taken into account.

With this in hand the full Hamiltonian of the system is found to be composed by a sum of four terms, the last two being interaction terms, where three or more

Parameter	Value	Description
$I_c$	5 $\mu$ A	Josephson critical current
$C_g$	14 fF	Ground capacitance
$L_g$	53 pH	Geometrical inductance
$C_J$	60 fF	Josephson capacitance
$a$	60 $\mu$ m	Unit cell length
$N$	900	Number of unit cells
$\omega_p$	$2\pi \cdot 12$ GHz	Pump frequency
$\omega_s$	$2\pi \cdot 5$ GHz	Signal frequency
$\omega_i$	$2\pi \cdot 7$ GHz	3WM idler frequency
$\omega_j$	$2\pi \cdot 19$ GHz	4WM idler frequency

Table I. Circuit parameters used for the numerical evaluations

modes give rise to 3WM or 4WM.

$\chi_1^{(n)}$  and  $\chi_0$  describe respectively the free field energy of the traveling modes and the magnetic energy stored into the rf-SQUIDS due to the magnetic field or DC current bias applied. Furthermore  $\chi_3^{(n,l,m)}$  and  $\chi_4^{(n,l,m,s)}$  are respectively the coupling parameters that characterize the 3WM and 4WM, both strongly dependent on the circuit parameters of the unit cell and on the frequency of the modes that populate the TWJPA. For the complete expression of the coupling coefficients as a function of the layout and experimental parameters see Appendix D. The distinctive characteristic of the layout under study is the strong dependence of these coupling parameters with respect to the external bias conditions, opening the possibility to properly select a working regime (3WM or 4WM). Each coupling parameter, defined by a set of indices (e.g.  $n$ ,  $l$ ,  $m$  and  $s$ ), quantifies the interaction strength of the respective modes. It is then clear that different combinations of indices represent different effects that take place into the TWJPA which contribute to the output field. If we now focus on a particular working regime of the amplifier it can be noted that if the TWJPA is biased so that the Kerr-like nonlinearity is suppressed, it is legit to consider the amplifier as a pure three-wave mixer, where the conservation of energy imposes the creation of the so-called Idler mode at frequency  $\omega_p - \omega$ , being  $\omega_p$  and  $\omega$  the Pump and Signal frequencies respectively. On the contrary, if the quadratic nonlinearity gets suppressed, the TWJPA becomes a pure four-wave mixer, hence, with the degenerate pump assumption valid since now on for the 4WM regime, the Idler will be located at  $2\omega_p - \omega$ .

### C. Gain and Squeezing in 3WM and 4WM

In order to analytically treat the problem the number of traveling modes that populate the TWJPA will be restricted to three, the input pump and signal frequencies plus the idler frequency that changes depending on the active nonlinearity. This assumption implies that mixed

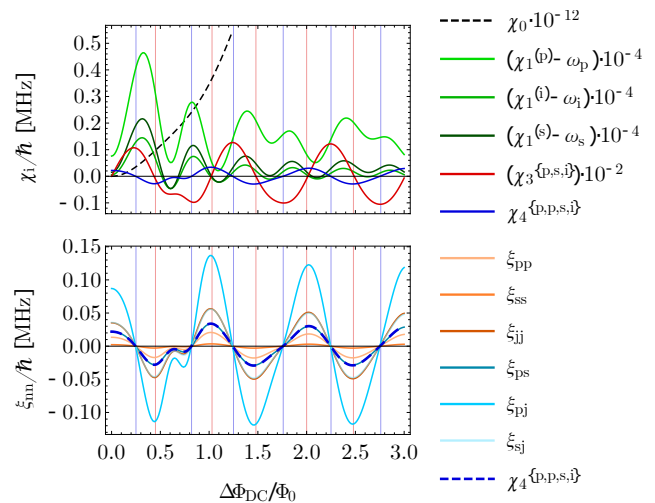


Figure 2. Hamiltonian coupling parameters  $\chi_i$  characterizing the Hamiltonian (10) versus the normalized DC flux bias ( $\Delta\Phi_{DC}/\Phi_0$ ). The Hamiltonian coefficient related to the constant flux bias ( $\chi_0$ ) has been scaled by a factor of  $10^{12}$  while the non-interacting-modes Hamiltonian coupling constants ( $\chi_1^{(n)}$ ) have been shifted by the frequency of the corresponding photon ( $\omega_i$ ) and scaled by a factor  $10^4$ . The indices in the superscripts vary with the considered mode and can take the values p (pump), s (signal) and i (idler). The blue vertical lines indicate the flux biases at which the amplifier works as a three-wave mixer (see Section II C for a detailed description), while the red vertical lines indicate the flux biases at which the amplifier works as a four-wave mixer. The coupling parameters  $\xi_{n,n}$  and  $\xi_{n,l}$  refer to the self-phase and cross-phase modulation due to the 4WM interaction. The circuit parameters used to perform the numerical evaluations and plots are summarized in table I.

3WM/4WM states will not be taken into account, because the presence of a mixed state would require a four coupled modes discussion, that goes beyond the scope of this paper. Furthermore, since now the 3WM regime will be considered in a non-degenerate condition, that is  $\omega \neq \omega_p/2$ . With this in hand the full Hamiltonian (10), can be reduced to two different forms depending on the regime the amplifier is working in. Concerning the 3WM, the following Hamiltonian is obtained

$$\begin{aligned} \hat{H}_{3WM} = & \hbar\chi_0 + \sum_{n=\{\omega_p, \omega, \omega_p-\omega\}} \hbar\chi_1^{(n)} \left( \hat{a}_n^\dagger \hat{a}_n + \frac{1}{2} \right) + \\ & + \hbar\chi_3^{\{\omega_p, \omega, \omega_p-\omega\}} \left( \hat{a}_{\omega_p}^\dagger \hat{a}_\omega \hat{a}_{\omega_p-\omega} + \hat{a}_\omega^\dagger \hat{a}_{\omega_p-\omega} \hat{a}_{\omega_p} \right) \end{aligned} \quad (11)$$

having introduced  $\chi_3^{\{\omega_p, \omega, \omega_p-\omega\}}$  as the sum of all the possible terms arising from index permutations of  $\chi_3^{(\omega_p, \omega, \omega_p-\omega)}$  neglecting permutations signs degeneracy.

While the 4WM Hamiltonian results to be

$$\begin{aligned} \hat{H}_{4\text{WM}} = & \hbar\chi_0 + \hbar\xi_0 + \sum_{n=\{\omega_p, \omega, 2\omega_p - \omega\}} \hbar\chi_1^{(n)} \left( \hat{a}_n^\dagger \hat{a}_n + \frac{1}{2} \right) + \\ & + \sum_{n=\{\omega_p, \omega, 2\omega_p - \omega\}} \hbar\xi_n \hat{a}_n^\dagger \hat{a}_n + \\ & + \sum_{n,l=\{\omega_p, \omega, 2\omega_p - \omega\}} \hbar\xi_{n,l} \hat{a}_n^\dagger \hat{a}_n \hat{a}_l^\dagger \hat{a}_l + \\ & + \hbar\chi_4^{\{\omega_p, \omega_p, \omega, 2\omega_p - \omega\}} \cdot \left( \hat{a}_{\omega_p}^\dagger \hat{a}_{\omega_p}^\dagger \hat{a}_\omega \hat{a}_{2\omega_p - \omega} + \hat{a}_\omega^\dagger \hat{a}_{2\omega_p - \omega}^\dagger \hat{a}_{\omega_p} \hat{a}_{\omega_p} \right) \quad (12) \end{aligned}$$

where  $\xi_0$  is a small correction to the zero-point energy,  $\xi_n$  is a small contribution to the free-field energy of the modes and  $\xi_{n,l}$  is the coefficient describing the self- ( $n = l$ ) and cross-phase ( $n \neq l$ ) modulation phenomena. All these latter arise from the 4WM interaction in the medium. Likewise the 3WM case,  $\chi_4^{\{\omega_p, \omega_p, \omega, 2\omega_p - \omega\}}$  is the sum of all the possible terms that derive from index permutations of  $\chi_4^{(\omega_p, \omega_p, \omega, 2\omega_p - \omega)}$  neglecting permutations signs degeneracy.

Figure 2 shows the behaviour of the most significant coupling parameters as a function of  $\Delta\Phi_{\text{DC}}$ . All these coefficients present an oscillating-like behaviour with multiple zeros for different values of  $\Delta\Phi_{\text{DC}}$  while red and blue vertical lines represent particular bias values (working points) that select the 4WM or 3WM working regimes respectively.

Once the Hamiltonian of the system is known, it is possible to work out the dynamic of the observables. Exploiting the Heisenberg picture of quantum mechanics, the time evolution of the creation and annihilation operators can be computed through the Heisenberg equation  $d\hat{a}_H(t)/dt = (i/\hbar)[\hat{H}, \hat{a}_H(t)] + (\partial\hat{a}_H/\partial t)_H$  (for the complete calculations see Appendix E). From here to the end of Section II C we will drop the H subscript.

A system of coupled equations (3WM (E1)-(E3), 4WM (E4)-(E6)) comes out, that is not exactly solvable analytically [26]. Indeed, one can proceed with the so-called *undepleted pump approximation* to analytically treat the system. Such an approximation requests the pump amplitude to be much higher than the signal and idler ones so that its magnitude does not change significantly during the interaction process. On the other hand, under the so-called *classical pump approximation*, the ladder operator describing the pump mode can be treated as a classical amplitude

$$\sqrt{\frac{2\hbar\omega_p}{C_g N}} \hat{a}_p \mapsto A_p \quad (13)$$

being  $A_p$  the classical voltage amplitude of  $\hat{V}_{C_g}$  (equation (4)).

The strong interplay between the traveling waves manifests itself in a system of coupled differential equations for the annihilation operators describing the signal and idler modes

$$\frac{d\hat{a}_\omega}{dt} = -i\Upsilon \hat{a}_\omega^\dagger e^{-i\Psi t} \quad (14a)$$

$$\frac{d\hat{a}_{\omega'}}{dt} = -i\Upsilon \hat{a}_\omega^\dagger e^{-i\Psi t} \quad (14b)$$

where the *density phase mismatch*  $\Psi$  has been defined (3WM - equation (E22), 4WM - equation (E15)). The main structure of the system stays the same regardless of the kind of interaction that takes place into the TWJPA, indeed it is possible to define an *interaction parameter*  $\Upsilon = \Upsilon_{3\text{WM}, 4\text{WM}}$  that characterizes the working regime the amplifier is biased in.

$$\Upsilon_{3\text{WM}} = \chi_3 |A_{p,0}| \quad (15a)$$

$$\Upsilon_{4\text{WM}} = \chi_4 |A_{p,0}|^2 \quad (15b)$$

$\chi_{3,4}$  are two bias tunable coefficients that incorporate information about the strength of the quadratic or cubic non-linearity into the device (for their definition refer to equations (E16) and (E23)). It has to be noticed that in  $\Upsilon_{3\text{WM}, 4\text{WM}}$  the proportionality to the initial pump amplitude  $A_{p,0}$  reflects the nature of the scattering taken into account, hence involving one (linear) or two (quadratic) pump photons.

Under the undepleted pump assumption and working in the co-rotating frame one can find the following analytical solution to equations (14a) and (14b)

$$\begin{aligned} \hat{a}_\omega(t) = & \left[ \hat{a}_{\omega,0} \left( \cosh(gt) + \frac{i\Psi}{2g} \sinh(gt) \right) - \right. \\ & \left. - \frac{i\Psi}{g} (\hat{a}_{\omega',0})^\dagger \sinh(gt) \right] e^{-i(\Psi/2)t} \quad (16) \end{aligned}$$

being  $\hat{a}_{\omega,0}$  and  $(\hat{a}_{\omega',0})^\dagger$  the ladder operators at the initial interaction time and with the *complex gain factor*

$$g = \sqrt{\Upsilon^2 - \left( \frac{\Psi}{2} \right)^2} \quad (17)$$

For the 3WM case, under experimentally reasonable parameter (see Table I) a *negligible total phase mismatch approximation*, hence the phase mismatch density times the interaction time, can be considered in equation (16), so that  $\Psi t \approx 0$  and the phase lag between the traveling modes can be neglected. Moreover, in the undepleted pump approximation it can be shown that the gain variation given by the phase mismatch density in (17) can be neglected since  $\Upsilon^2 \gg \frac{\Psi^2}{4}$ , giving the much simpler relation

$$g \approx |\Upsilon_{3\text{WM}}| \quad (18)$$

It is helpful to introduce a set of auxiliary functions that incorporates the behaviour of the TWJPA and simplifies the notation

$$u(\omega, t) = \cosh(g(\omega)t) + \frac{i\Psi(\omega)}{2g(\omega)} \sinh(g(\omega)t) \quad (19)$$

$$v(\omega, t) = -\frac{\Upsilon}{g(\omega)} \sinh(g(\omega)t) \quad (20)$$

It is now possible to define the gain of a TWJPA as the ratio among the average number of photons of frequency  $\omega$  after a certain amount of time  $t$  spent into the medium and the average number of photons at the same frequency entering the transmission line

$$G(\omega) = \frac{\langle \hat{a}_\omega^\dagger \hat{a}_\omega \rangle}{\langle (\hat{a}_{\omega,0})^\dagger \hat{a}_{\omega,0} \rangle} = |u|^2 + \frac{|v|^2 [\langle (\hat{a}_{\omega',0})^\dagger \hat{a}_{\omega',0} \rangle + 1] + iu^*v\langle (\hat{a}_{\omega,0})^\dagger (\hat{a}_{\omega',0})^\dagger \rangle - iuv^*\langle \hat{a}_{\omega',0} \hat{a}_{\omega,0} \rangle}{\langle (\hat{a}_{\omega,0})^\dagger \hat{a}_{\omega,0} \rangle} \quad (21)$$

Equation (21) is a general relation to estimate the number of outgoing signal photons regardless of the nature of the incoming state (Fock, coherent, thermal, etc.). The classical limit of equation (21) can be found by setting a large amount of input signal photons, hence  $\langle (\hat{a}_{\omega,0})^\dagger \hat{a}_{\omega,0} \rangle \gg 1$  and by setting the number of input idler photons to zero, so  $\langle (\hat{a}_{\omega',0})^\dagger \hat{a}_{\omega',0} \rangle \approx 0$

$$G(\omega) \approx |u|^2 \approx 1 + \sinh^2 gt \quad (22)$$

that results to be in accordance with [16]. Moreover, it is possible to explicitly compute the gain for an incoming Fock state  $|\Psi\rangle = |n_\omega, n_{\omega'}\rangle$  or a coherent state  $|\Psi\rangle = |\alpha_\omega, \beta_{\omega'}\rangle$  starting from equation (21)

$$G_{F,H} = |u|^2 + \frac{n_{\omega'} + 1}{n_\omega} |v|^2 \quad (23)$$

$$G_{C,H} = |u|^2 + \frac{(|\beta_{\omega'}|^2 + 1)|v|^2 + iu^*v\alpha_\omega^*\beta_{\omega'}^* - iuv^*\alpha_\omega\beta_{\omega'}}{|\alpha_\omega|^2} \quad (24)$$

Figure 3(a) shows several plots of equation (23) calculated for Fock input states with different numbers of signal photons and for the experimental parameters reported in Table I. It is evident that the quantum gain of (23) tends to (22) for a large number of input photons ( $n_\omega > 64$ ). Moreover, a closer look at the curves representing equation (22) with and without negligible phase mismatch shows that the approximation  $\Psi \approx 0$  holds in all the bandwidth only for the 3WM regime. The orange, red and blue curves are plotted for growing pump powers, hence the gain, which shows a maximum at half the pump frequency, is strongly dependent on the pumping power.

The correlation of the signal and idler photons results in a squeezed output field of the TWJPA. In order to

model these correlations one can introduce quadratures as

$$\hat{Y}^\theta(\omega) = i(e^{i\theta/2}\hat{a}_\omega^\dagger - e^{-i\theta/2}\hat{a}_\omega) \quad (25)$$

with their associated fluctuations

$$\Delta\hat{Y}^\theta(\omega) = \hat{Y}^\theta(\omega) - \langle \hat{Y}^\theta(\omega) \rangle \quad (26)$$

being  $\theta$  the so-called squeezing angle.

From the previous definitions one can compute (see Appendix F) the relation between the squeezing spectrum  $S$  and the quadratures fluctuations as

$$S(\omega) = \int_0^\infty d\omega' \langle \Delta\hat{Y}^\theta(\omega) \Delta\hat{Y}^\theta(\omega') \rangle \quad (27)$$

For a vacuum input state, it can be shown that the product of the fluctuations of the two quadratures gives the minimum possible value allowed by the Heisenberg uncertainty principle, fingerprint of a quantum limited amplification [27]. From (27) the squeezing spectrum is then

$$S(\omega) = 1 + 2|v(\omega, t)|^2 - 2|v(\omega, t)|\sqrt{|v(\omega, t)|^2 + 1} \quad (28)$$

Figure 3(b) shows the squeezing spectrum of equation (28) plotted as a function of the signal frequency for different input pump powers, calculated for a vacuum input state. The squeezing spectrum shows a minimum at half the pump frequency, just like the gain, that become more pronounced with a stronger pump power.

#### D. Interaction of quantum states through 3WM or 4WM

The time evolution of the state vectors can give important hints on the behaviour of the TWJPA in pres-

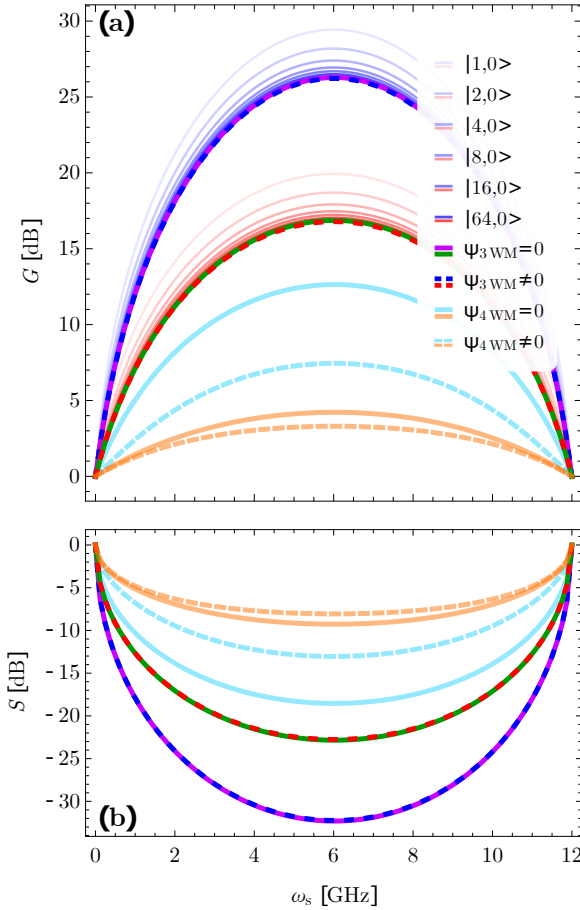


Figure 3. (a) Gain  $G$  of the TWJPA under the undepleted pump approximation expressed by equation (22) and (23) in the 4WM (light blue/orange) and 3WM (blue,red) regimes. Several curves with and without zero phase mismatch, respectively  $\Psi = 0$  and  $\Psi \neq 0$ , are presented. The lighter curves are calculated considering a different number of input signal photons for Fock states, while the purple and green indicate the classical limit, expressed by equation (22) for  $P_p = -50$  dBm and  $P_p = -46$  dBm respectively. (b) Squeezing spectrum  $S$  (equation (28)) as a function of the signal frequency calculated for a vacuum input state in the 4WM and 3WM regimes. Different colors express different pump powers ( $P_p$ ) for which  $G$  and  $S$  are calculated: blue/light blue  $P_p = -50$  dBm, red/orange  $P_p = -46$  dBm.

ence of single photon level signals. Moving to the framework of the interaction picture it is possible to calculate the output photon statistics in the Fock base for any incoming state. The time evolution of a quantum state  $|\psi(t)\rangle$  can be expressed as

$$|\psi(t)\rangle = e^{-\frac{i}{\hbar} \int_0^t \hat{H}_{\text{int}} dt'} |\psi(0)\rangle = e^{-\frac{i}{\hbar} \hat{H}_{\text{int}} t} |\psi(0)\rangle \quad (29)$$

where  $\hat{H}_{\text{int}} = \hat{H}_{\text{int},3\text{WM}}(4\text{WM})$  is the three(four)-wave mixing Hamiltonian written in the co-rotating frame, under the undepleted pump approximation:

$$\hat{H}_{\text{int},3\text{WM}} = \hbar \chi_3 |A_{p,0}| \left( \hat{a}_s \hat{a}_i e^{i\Psi t} + \hat{a}_s^\dagger \hat{a}_i^\dagger e^{-i\Psi t} \right) \quad (30)$$

$$\hat{H}_{\text{int},4\text{WM}} = \hbar \chi_4 |A_{p,0}|^2 \left( \hat{a}_s \hat{a}_i e^{i\Psi t} + \hat{a}_s^\dagger \hat{a}_i^\dagger e^{-i\Psi t} \right) \quad (31)$$

Under the negligible phase mismatch condition (i.e.,  $\Psi t \ll 1$ ) equation (29) becomes

$$|\psi(t)\rangle = e^{i\kappa(\hat{a}_s \hat{a}_i + \hat{a}_s^\dagger \hat{a}_i^\dagger)} |\psi(0)\rangle \quad (32)$$

where  $\kappa = -\chi_3 |A_{p,0}| t$  ( $\kappa = -\chi_4 |A_{p,0}|^2 t$ ) is the amplification factor for the 3WM (4WM) regime. Equation (32) can be written in a normal ordered form as

$$|\psi(t)\rangle = e^{i \tanh(\kappa) \hat{a}_s^\dagger \hat{a}_i^\dagger} \cdot e^{-\ln[\cosh(\kappa)](1 + \hat{a}_s^\dagger \hat{a}_s + \hat{a}_i^\dagger \hat{a}_i)} \cdot e^{i \tanh(\kappa) \hat{a}_s \hat{a}_i} |\psi(0)\rangle \quad (33)$$

In the following, the time evolution of two different classes of initial input states will be analyzed.

### 1. Fock States input

This subsection focus on the characteristics of the time-evolution of an initial Fock state  $|\psi_{F(0)}\rangle = |N_{\text{in}}^S\rangle_s |N_{\text{in}}^I\rangle_i$ . Starting from equation (33) and considering their action on the initial state, by means of a power expansion of each exponential function, the expression of the quantum state at a certain time  $t$  can be derived. Then, the expectation value of the signal photon number operator  $\hat{n}_s = \hat{a}_s^\dagger \hat{a}_s$  on the final state  $|\psi_{F(t)}\rangle$  can be expressed as

$$\langle \hat{n}_s \rangle_{\psi_{F(t)}} = \langle \psi_{F(t)} | \hat{n}_s | \psi_{F(t)} \rangle = \sum_{N_{\text{fin}}^S} P_F(N_{\text{fin}}^S) \cdot N_{\text{fin}}^S \quad (34)$$

where  $P_F(N_{\text{fin}}^S)$  is the probability to measure  $N_{\text{fin}}^S$  signal photons in the final state, and  $N_{\text{in}}^S - \min\{N_{\text{in}}^S, N_{\text{in}}^I\} < N_{\text{fin}}^S < \infty$ . This probability distribution can be expressed by exploiting the binomial coefficients as a function both of the characteristics of the initial state and of the characteristics of the medium

$$P_F = \sum_{n,n'=0}^{\min\{N_{\text{in}}^S, N_{\text{in}}^I\}} \frac{(-1)^{n-n'} [\tanh(\kappa)]^{2(N_{\text{fin}}^S - N_{\text{in}}^S + n + n')}}{[\cosh(\kappa)]^{2(1 + N_{\text{in}}^S + N_{\text{in}}^I - n - n')}} \cdot \binom{N_{\text{in}}^S}{n'} \binom{N_{\text{in}}^I}{n} \binom{N_{\text{fin}}^S}{N_{\text{in}}^S - n} \binom{N_{\text{fin}}^S - N_{\text{in}}^S + N_{\text{in}}^I}{N_{\text{in}}^I - n'} \quad (35)$$

In figure (4) the time evolution of the probability distribution is represented for three different initial

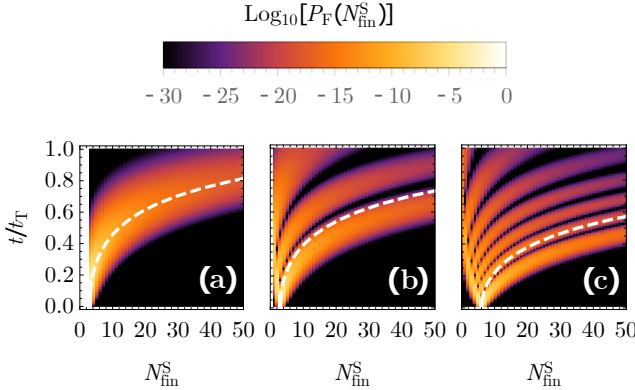


Figure 4. Time evolution inside the medium, from its input port ( $t = 0$ ) to the output port ( $t = t_T$ ) of the probability distribution  $P_F$  to find  $N_{\text{fin}}^S$  signal photons for three different initial Fock states (a)  $|3\rangle_s|0\rangle_i$ , (b)  $|3\rangle_s|2\rangle_i$  and (c)  $|6\rangle_s|6\rangle_i$ . The dashed white lines represent the time evolution of the expectation value  $\langle \hat{n}_s \rangle$

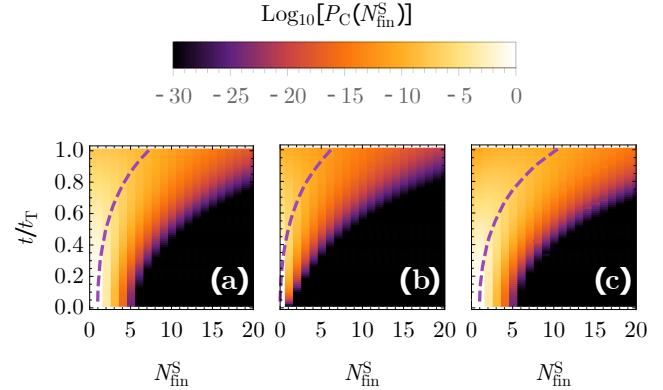


Figure 5. Time evolution inside the medium, from its input port ( $t = 0$ ) to the output port ( $t = t_T$ ) of the probability distribution  $P_C$  to find  $N_{\text{fin}}^S$  signal photons for two different initial bimodal coherent states  $|\alpha\rangle_s|\beta\rangle_i$ . (a)  $|1\rangle_s|0\rangle_i$ , (b)  $|0\rangle_s|1\rangle_i$ , and (c)  $|1\rangle_s|1\rangle_i$ . The dashed purple lines represent the time evolution of the expectation value  $\langle \hat{n}_s \rangle$

number states, for a 3WM interaction and for the experimental parameters reported in Table I. In all cases, at the beginning of the interaction, the probability distribution is single-peaked and has a maximum in correspondence of  $N_{\text{in}}^S$ . Then, due to the non-linearity of the system, the distribution can turn into a multi-peaked distribution if  $N_{\text{in}}^I \neq 0$ . In this case the distance between peaks increases with the time. After the initial transition time, the number of maximum becomes constant and equal to  $\min\{N_{\text{in}}^S, N_{\text{in}}^I\} + 1$ . This value reflects the number of possible combinations that can occur between the initial signal and idler photons at the beginning of the interaction. Considering the case of an initial state  $|3\rangle_s|2\rangle_i$  (Fig. 4(b)), at  $t = 0$  and with a certain probability, two couple of signal-idler photons may recombine to create a pair of pump photons. This leads to the *effective* propagation and amplification of a single remaining signal photon. Yet, with a different given probability, just a single couple of signal-idler photons or none of them recombine, leading to the *effective* propagation and amplification of, respectively, two or three signal photons. In addition, considering Fig. 4(c) it can be noted that in the case of  $N_{\text{in}}^S = N_{\text{in}}^I$ , despite the fact that  $N_{\text{in}}^S \neq 0$ , the probability to observe at the end of the amplifier  $N_{\text{fin}}^S = 0$  is significantly non-zero. This is in accordance with the fact that an *effective* propagation and amplification of the vacuum state can occur.

Furthermore, exploiting the definition given in equation (34), and consistently with equation (23), a quan-

tum definition of the gain of the amplifier can be given

$$G_{F,I} = \frac{\langle \hat{n}_s \rangle_{\psi_F(t)}}{\langle \hat{n}_s \rangle_{\psi_{F(0)}}} = \frac{\langle \hat{n}_s \rangle_{\psi_F(t)}}{N_{\text{in}}^S} \quad (36)$$

## 2. Coherent States input

Similarly to what has been performed in the case of a Fock state input, the expectation value of the signal photon number operator can be derived by (34) considering an initial bimodal coherent state  $|\psi_c(0)\rangle = |\alpha\rangle_s|\beta\rangle_i$  and having the following probability distribution

$$P_C = \sum_{m,n,n'=0}^{\infty} \frac{(-1)^{n-n'} [\tanh(\kappa)]^{n+n'}}{[\cosh(\kappa)]^{2(1+N_{\text{fin}}^S+m-n')}} \cdot \frac{\alpha^{N_{\text{fin}}^S-n} (\alpha^*)^{N_{\text{fin}}^S-n'} \beta^m (\beta^*)^{m+n-n'}}{e^{[|\alpha|^2+|\beta|^2+i(\alpha^*\beta^*-\alpha\beta)\tanh(\kappa)]}} \cdot \frac{1}{m! (N_{\text{fin}}^S-n)!} \binom{N_{\text{fin}}^S}{n} \binom{m+n}{n'} \quad (37)$$

The time evolution of the probability distribution  $P_C$  is presented in figure (5) for three different initial bimodal coherent states. In contrast with  $P_F$ , this distribution is always single-peaked over the whole range of the interaction and its maximum shifts in time starting from  $N_{\text{fin}}^S = |\alpha|^2$ . It can also be noticed that, for a fixed  $\alpha$ , the distribution becomes wider and wider with the increase of  $\beta$ .

In this case again, the quantum gain of the amplifier results to be consistent with the equation found in the

Heisenberg picture (24) and can be expressed as

$$G_{C,I} = \frac{\langle \hat{n}_s \rangle_{\psi_c(t)}}{\langle \hat{n}_s \rangle_{\psi_c(0)}} = \frac{\langle \hat{n}_s \rangle_{\psi_c(t)}}{|\alpha|^2} \quad (38)$$

### III. DISCUSSIONS

#### A. Experimental constraints and impedance matching

In order to couple the TWJPA with its electromagnetic environment a particular (e.g.  $Z_c = 50 \Omega$ ) impedance matching is commonly required. This target can be reached with non-trivial additional on-chip components or by properly tuning the cells parameters. This subsection is devoted to the search for a set of parameters that fulfill this aim by expressing all the other cell parameters as a function of  $I_c$ . For simplicity and without lacking of generality, in the following  $C_J$  is supposed to be constant.

In order to keep the induced magnetic flux function into the rf-SQUID single valued, a design characterized by a screening parameter  $\beta$ , given by

$$\beta = \frac{2\pi L_g I_c}{\phi_0} < 1 \quad (39)$$

is required. It is evident that a certain  $\beta$  set a hyperbolic relation between  $L_g$  and  $I_c$ .

For a generic mode  $n$ , an expression for  $C_g$  having set  $I_c$  (consequently  $L_g$ ) and  $Z_c$  can be inferred starting from the relation for the characteristic impedance of a lossless transmission line ( $Z_n = \sqrt{L_n/C_g^n}$ )

$$C_g^n = \frac{L_n}{Z_n^2} = \frac{1}{Z_n^2} \frac{\Lambda_n L_g}{1 + \Lambda_n \frac{L_g}{L_J}} = \frac{\frac{L_g}{1 - L_g C_J \omega_n^2}}{Z_n^2 \left( 1 + \frac{1}{1 - L_g C_J \omega_n^2} \frac{L_g}{\frac{\varphi_0}{I_c} \sin \Delta \Phi / \varphi_0} \right)} \quad (40)$$

It has to be noticed that the impedance matching can be achieved just for a single mode since the characteristic impedance  $Z_n$  of the line is frequency dependant. The matched mode can be engineered *ad-hoc* depending on the experiment requirements. If a low power reflection is mandatory, the matched mode should be the pump, instead, if no signal loss is preferred the signal mode should be the matched one.

Figure 6(a) reports several curves representing the trends given by equations (39) and (40) plotted as functions of  $I_c$  for different values of  $\beta$  and for a  $50 \Omega$  matching of a signal at 5 GHz.

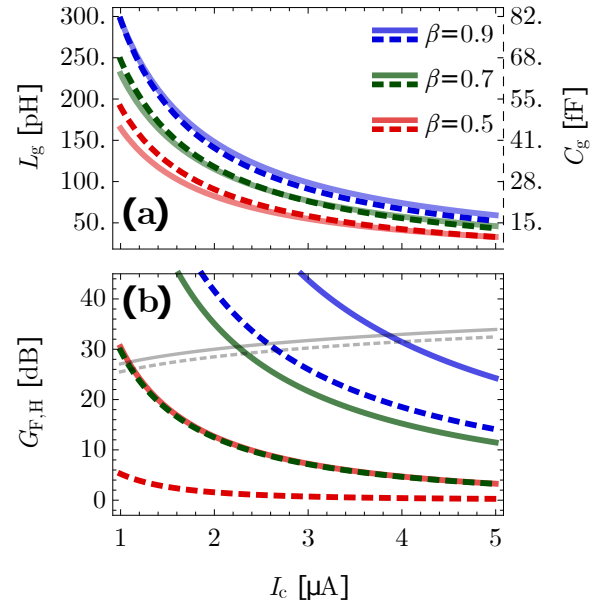


Figure 6. (a) The plot shows three sets of curves calculated for different values of the screening parameter  $\beta$  representing the cell parameters for a  $50\Omega$  matching of the signal mode at 5 GHz as a function of the critical current  $I_c$ . The full curves refer to the left axis and reports the geometrical inductance ( $L_g$ ) vs.  $I_c$ . On the contrary, the dashed curves refer to the right axis and represents the ground capacitance ( $C_g$ ) vs.  $I_c$ . (b) The figure shows the gain  $G_{F,H}$  of the TWJPA in 3WM mode (full curves) and 4WM mode (dashed curves) as a function of the critical current  $I_c$  for different values of the screening parameter  $\beta$ . The ground capacitance  $C_g$  and the geometrical inductance  $L_g$  are fixed for every value of  $I_c$  by the  $50\Omega$  matching condition (40) and by the value of  $\beta$  (39). Below the grey curves given by (42) the undepleted pump approximation holds.

#### B. Validity of the undepleted pump approximation

In order to obtain equations (14a) and (14b) the undepleted pump approximation has been made. Physically speaking this means that from there on the pump power should be considered much higher than the signal and idler ones. This boundary directly translates into a common relation for the number of pump photons into the amplifier, that must be always at least 10 times higher than the other modes.

$$n_p > 10 \cdot n_{s,i} \quad (41)$$

Equation (41) is nothing but a condition on the modes powers that has been recast using the number of photons. Exploiting the definition of gain (21) and substituting the operators with their expectation val-

ues, (41) becomes

$$\begin{aligned} n_s &< \frac{n_p}{10} \\ Gn_{s,0} &< \frac{n_p}{10} \\ G &< \frac{1}{10} \frac{n_p}{n_{s,0}} \end{aligned} \quad (42)$$

the latter being a simple but powerful constraint on the maximum gain that the amplifier can express remaining well described by the undepleted pump approximation. This condition is very general because it just depends on the ratio between the number of pump photons and the number of incoming signal photons setting the limit at which the signal photonic population reaches the same order of magnitude than the pump one, hence the rate of annihilation of pump photons due to the generation of signal ones is no longer negligible. This limit is represented in figure 6(b) by the grey curves that cut the gain for a single photon Fock input state given by (23). For the screening parameter  $\beta$  approaching unity the gain functions loose validity for higher values of the critical current because the non-linearity related to the induced flux into the rf-SQUID gets stronger. For lower values of  $\beta$  the range of validity gets extended and the gain functions remain valid for lower critical currents.

### C. Model validity due to Taylor expansions

In subsection II B two different Taylor expansions were performed regarding the Josephson energy into (3) and the nonlinear flux operator (9). In both expansions the phase swing  $\delta\Phi$  is considered to be small, reflecting the amplitude of the AC current flowing into the transmission line. For this reason, it is necessary to point out the limit of validity of the model in terms of phase swing, hence of current. Since the pump current is considered to be much higher of the signal and idler ones (undepleted and classical pump approximations) it is legit to consider all the current flowing into the TWJPA equal to the pump current  $I_p$ . This fact means that, for the model to be valid,  $I_p$  needs to be smaller than a certain threshold.

An error function can be built for the Josephson energy and equation (9) as the difference between the real function and its series expansion. The threshold is then chosen so that the error functions are always smaller than 5%, for any  $I_p$  used during the computations.

Figure 7 shows the error functions calculated for equation (9) (solid lines) and (3) (dashed lines) for values of  $\Delta\Phi_{DC}$  corresponding to the 3WM and 4WM working points. It can be seen that the limits on the pump current are non symmetric respect to the origin.

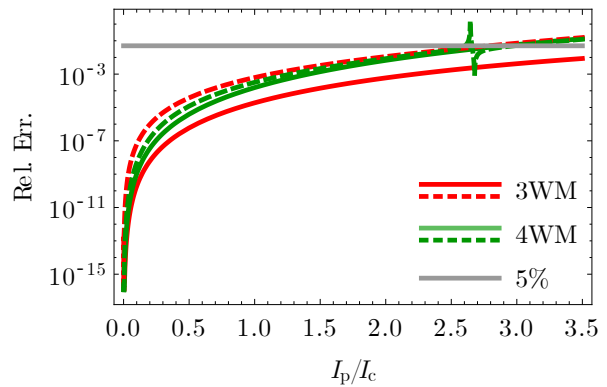


Figure 7. The solid curves represent the error function of (9) while the dashed curves indicate the error function of the Josephson energy into (3). The error functions are calculated as the relative difference between the function and its Taylor expansion versus the normalized AC pump ( $I_p/I_c$ ) calculated in the 4WM and 3WM working points. The horizontal gray line indicates the 5% threshold chosen as the reference error.

This fact seems to tell that there could be a preferential direction that allow to feed the amplifier with more current, however it is clear that this asymmetry is just given by the lack of parity of the expanded functions, that therefore extend for different ranges their validity for positive or negative pump currents. For any practical purposes the strictest limit needs to be considered since the fluctuations of the phase swing (hence of the pump current) are symmetric respect to the origin. This fixes the maximum pump current allowed by the model. It's worth mentioning that the resonances in the 4WM curves arise from the  $I_p$  values for which the Josephson inductance diverges.

## IV. CONCLUSIONS

A quantum theory for the parametric amplification via a chain of rf-SQUIDS embedded in a wave-guide has been developed through a circuit-QED approach. A mixed lumped/distributed-element approach has been adopted in order to define the Hamiltonian of the system, valid for both 3WM and 4WM interactions. The dynamics of the system has been calculated first in the Heisenberg picture where, through the solution of a system of Quantum Langevin Equations for the traveling modes, a closed form for the evolution of the photonic populations, power gain and squeezing spectrum were found. Then, by means of the interaction picture, the time evolution of some representative input states (Fock and coherent states) has been calculated, allowing to model the quantum dynamics of photonic amplification and recombination into the TWJPA in the few ph-

tons regime. The closed forms derived for the transmission line parameters represents simple constraints on the unit cell circuit components, so that the model validity has been linked to a clear experimental parameter space.

## ACKNOWLEDGMENTS

This work has been partially funded by the SUPERGALAX project in the framework of the H2020-FETOPEN-2018-2020 call and the Joint Research Project PARAWAVE of the European Metrology Programme for Innovation and Research (EMPIR). This project has received funding from the EMPIR programme co-financed by the Participating States and from the European Unions Horizon 2020 research and innovation programme.

## AUTHOR CONTRIBUTION

A.G., L.F., E.E. and L.C. conceptualized the work. A.G., L.F. and E.E. carried out the theoretical and numerical analysis. A.G., L.F. and E.E. wrote the manuscript. L.C. and A.M. participated in the discussion and editing of the manuscript.

## Appendix A: Hamiltonian linear density of the elementary cell components

In this appendix we start describing the general method used to calculate the energy stored in a circuit element, then we derive the energy stored in each element which constitutes an elementary cell of a TWJPA. Defining  $I$  as the current flowing through a certain circuit element and  $V$  as the voltage drop across it, the energy stored in the electrical component at a certain time  $t$  can be expressed as the time-integrated power  $P = VI$ :

$$U(t) = \int_{t_0}^t P(t') dt' = \int_{t_0}^t I(t') \cdot V(t') dt' \quad (\text{A1})$$

The current flowing through a generic inductance  $L$  induces a magnetic flux  $\Delta\Phi(t) = LI(t)$ , and can be related to the voltage drop across the element by the relation

$$V(t) = L \frac{dI(t)}{dt} \quad (\text{A2})$$

Hence one can express the energy stored in the geo-

metrical inductance  $L_g$  as

$$\begin{aligned} U_{L_g}(t) &= \int_{t_0}^t I_{L_g}(t') \cdot V_{L_g}(t') dt' = \int_{t_0}^t I_{L_g}(t') \cdot L_g \frac{dI_{L_g}}{dt'} dt' \\ &= \frac{L_g}{2} I_{L_g}^2(t) = \frac{L_g}{2} \left( \frac{\Delta\Phi(t)}{L_g} \right)^2 = \frac{(\Delta\Phi(t))^2}{2L_g} \end{aligned} \quad (\text{A3})$$

having assumed  $I_{L_g}(t_0) = 0$ .

Exploiting the relation between magnetic flux difference and voltage drop

$$V(t) = \frac{d\Delta\Phi(t)}{dt} \quad (\text{A4})$$

the energy stored in the nonlinear Josephson inductance  $L_J$  can be expressed as

$$\begin{aligned} U_{L_J}(t) &= \int_{t_0}^t I_{L_J}(t') \cdot V_{L_J}(t') dt' \\ &= \int_{t_0}^t I_c \sin \left( \frac{\Delta\Phi(t')}{\varphi_0} \right) \cdot \frac{d\Delta\Phi(t')}{dt'} dt' \\ &= \varphi_0 I_c \left( 1 - \cos \left( \frac{\Delta\Phi(t)}{\varphi_0} \right) \right) \end{aligned} \quad (\text{A5})$$

having assumed  $\Delta\Phi(t_0) = 0$ .

Exploiting the relation between the current flowing through a capacitance  $C$  and the voltage drop  $V$  across its terminals

$$I(t) = C \frac{dV(t)}{dt} \quad (\text{A6})$$

the energy stored in the ground capacitance  $C_g$  can be expressed as

$$\begin{aligned} U_{C_g}(t) &= \int_{t_0}^t I_{C_g}(t') \cdot V_{C_g}(t') dt' \\ &= \int_{t_0}^t C_g \frac{dV_{C_g}(t')}{dt'} \cdot V_{C_g}(t') dt' \\ &= \frac{C_g}{2} V_{C_g}^2(t) = \frac{1}{2C_g} Q_{C_g}^2 \end{aligned} \quad (\text{A7})$$

having assumed  $V_{C_g}(t_0) = 0$ .

Lastly, exploiting relations (A4) and (A6), the energy stored in the capacitance associated to the Josephson junction can be expressed as

$$\begin{aligned} U_{C_J}(t) &= \int_{t_0}^t I_{C_J}(t') \cdot V_{C_J}(t') dt' \\ &= C_J \int_{t_0}^t \frac{d}{dt'} \left[ \frac{d\Delta\Phi(t')}{dt'} \right] \cdot \frac{d\Delta\Phi(t')}{dt'} dt' \\ &= \frac{C_J}{2} \left( \frac{d\Delta\Phi(t)}{dt} \right)^2 \end{aligned} \quad (\text{A8})$$

having assumed  $\Delta\Phi(t_0) = 0$ .

Using a standard procedure [25], one can derive the Hamiltonian operator that describes an electrical circuit starting from the definition of the energy stored in each of its components and transforming the physical observables into the corresponding operators. Furthermore, being  $a$  as the unit cell length, one can express the linear density of Hamiltonian associated to each component of the circuit represented in Figure 1 as

$$\hat{\mathcal{H}}_{L_g} = \frac{1}{2aL_g} \Delta\hat{\Phi}^2 \quad (\text{A9})$$

$$\hat{\mathcal{H}}_{L_J} = \frac{\varphi_0 I_c}{a} \left( 1 - \cos \left( \frac{\Delta\hat{\Phi}}{\varphi_0} \right) \right) \quad (\text{A10})$$

$$\hat{\mathcal{H}}_{C_g} = \frac{C_g}{2a} \hat{V}_{C_g}^2 = \frac{1}{2aC_g} \hat{Q}_{C_g}^2 \quad (\text{A11})$$

$$\hat{\mathcal{H}}_{C_J} = \frac{C_J}{2a} \left( \frac{\partial \Delta\hat{\Phi}}{\partial t} \right)^2 \quad (\text{A12})$$

## Appendix B: Inductance of the unit cell

It is useful to define an effective inductance that takes into account the parallel effect of the geometric inductance  $L_g$  and the Josephson capacitance  $C_J$ . Keeping in mind that the impedance of an inductor  $L$  for the mode  $n$  is  $Z_L = j\omega_n L$  while the impedance of a capacitor  $C$  for the same mode is  $Z_C = 1/j\omega_n C$ , we can write

$$\begin{aligned} \frac{1}{Z_{L_{\text{eff}},n}} &= \frac{1}{Z_{L_g}} + \frac{1}{Z_{C_J}} \\ \frac{1}{j\omega_n L_{\text{eff}},n} &= \frac{1}{j\omega_n L_g} + j\omega_n C_J \\ \frac{1}{L_{\text{eff}},n} &= \frac{1}{L_g} - \omega_n^2 C_J = \frac{1 - \omega_n^2 L_g C_J}{L_g} \end{aligned} \quad (\text{B1})$$

It is found that the dispersion coefficient of the  $n$ -th mode ( $\Lambda_n$ ) can be defined by the relation

$$L_{\text{eff},n} = \frac{L_g}{1 - \omega_n^2 L_g C_J} \equiv \Lambda_n L_g \quad (\text{B2})$$

It is now possible to compute the total inductance of the elementary cell by calculating the parallel of the effective inductance  $L_{\text{eff},n}$  and the Josephson inductance  $\hat{L}_J$

$$\frac{1}{\hat{L}_n} = \frac{1}{\hat{L}_J} + \frac{1}{L_{\text{eff},n}} = \frac{\hat{L}_J L_{\text{eff},n}}{\hat{L}_J + L_{\text{eff},n}} \quad (\text{B3})$$

Hence using equations (B2) and (6) the unit cell inductance can be written as

$$\begin{aligned} \hat{L}_n &= \frac{L_{J_0} L_g \left( \Delta\hat{\Phi}/\varphi_0 \right)}{L_{J_0} \left( \Delta\hat{\Phi}/\varphi_0 \right) \left( \frac{L_g}{L_{J_0}} \frac{\sin(\Delta\hat{\Phi}/\varphi_0)}{(\Delta\hat{\Phi}/\varphi_0)} + 1 - L_g C_J \omega_n^2 \right)} \\ &= \frac{L_g}{\frac{L_g}{L_{J_0}} \frac{\sin(\Delta\hat{\Phi}/\varphi_0)}{(\Delta\hat{\Phi}/\varphi_0)} + 1 - L_g C_J \omega_n^2} \\ &= \frac{\Lambda_n L_g}{1 + \Lambda_n \frac{L_g}{L_{J_0}} \frac{\sin(\Delta\hat{\Phi}/\varphi_0)}{(\Delta\hat{\Phi}/\varphi_0)}} \end{aligned} \quad (\text{B4})$$

## Appendix C: Nonlinear time-dependent flux operator

The nonlinear time-dependent component of the flux difference operator can be found through the constitutive equation of an inductor (8), where a mode decomposition has been performed. It has to be noticed that the inductance can be mode-dependent. The current through the unit cell can be calculated exploiting the telegrapher's equation (5), where the voltage drop to ground comes from (4) and the cell inductance of the  $n$ -th mode is found from equation (B4). Hence, the AC current passing through the line results to be

$$\hat{I}(z, t) = \sum_n \text{sgn}(n) \sqrt{\frac{\hbar\omega_n}{2\hat{L}_n N}} \left( \hat{a}_n e^{i(k_n z - \omega_n t)} + \text{H.c.} \right) \quad (\text{C1})$$

the nonlinear time-dependent flux operator  $\delta\hat{\Phi}$  is then

$$\begin{aligned} \delta\hat{\Phi} &= \sum_n \text{sgn}(n) \sqrt{\frac{\hbar\omega_n}{2\hat{L}_n N}} \hat{L}_n \left( \hat{a}_n e^{i(k_n z - \omega_n t)} + \text{H.c.} \right) \\ &= \sum_n \text{sgn}(n) \sqrt{\frac{\hbar\omega_n}{2N}} \sqrt{\Lambda_n L_g} \cdot \\ &\quad \cdot \left( 1 + \Lambda_n \frac{L_g}{L_{J_0}} \frac{\sin \frac{\Delta\Phi_{\text{DC}} + \delta\hat{\Phi}}{\varphi_0}}{\frac{\Delta\Phi_{\text{DC}} + \delta\hat{\Phi}}{\varphi_0}} \right)^{-1/2} \cdot \\ &\quad \cdot \left( \hat{a}_n e^{i(k_n z - \omega_n t)} + \text{H.c.} \right) = \\ &= \sum_n \left( 1 + \Lambda_n \frac{L_g}{L_{J_0}} \frac{\sin \frac{\Delta\Phi_{\text{DC}} + \delta\hat{\Phi}}{\varphi_0}}{\frac{\Delta\Phi_{\text{DC}} + \delta\hat{\Phi}}{\varphi_0}} \right)^{-1/2} \delta\hat{\Phi}_n^{(0)} \end{aligned} \quad (\text{C2})$$

where we have identified

$$\begin{aligned} \delta\hat{\Phi}_n^{(0)} &\equiv \text{sgn}(n) \sqrt{\frac{\hbar\omega_n}{2N}} \sqrt{\Lambda_n L_g} \left( \hat{a}_n e^{i(k_n z - \omega_n t)} + \text{H.c.} \right) \\ &= c_n \left( \hat{a}_n e^{i(k_n z - \omega_n t)} + \text{H.c.} \right) \end{aligned} \quad (\text{C3})$$

with

$$c_n = \text{sgn}(n) \sqrt{\frac{\hbar\omega_n}{2N}} \sqrt{L_g \Lambda_n}$$

Equation (C2) is a recursive relation that involves  $\hat{\delta\Phi}$  and can be solved imposing a solution to the lowest perturbative order, hence making the substitution  $\delta\hat{\Phi} \mapsto \delta\hat{\Phi}^{(0)} = \sum_n \delta\hat{\Phi}_n^{(0)}$  on the right hand side, so that we get

$$\delta\hat{\Phi} = \sum_n \left[ \left( 1 + \Lambda_n \frac{L_g}{L_{J_0}} \frac{\sin \frac{\Delta\Phi_{DC} + \delta\hat{\Phi}^{(0)}}{\varphi_0}}{\frac{\Delta\Phi_{DC} + \delta\hat{\Phi}^{(0)}}{\varphi_0}} \right)^{-1/2} \delta\hat{\Phi}_n^{(0)} \right] \quad (\text{C4})$$

By invoking the Taylor expansion of the square root into equation (C4) for  $\delta\hat{\Phi}^{(0)} \ll \varphi_0$ , one obtains

$$\delta\hat{\Phi} = \sum_n \left[ q_{0,n} + q_{1,n} \left( \delta\hat{\Phi}^{(0)} \right) + q_{2,n} \left( \delta\hat{\Phi}^{(0)} \right)^2 + q_{3,n} \left( \delta\hat{\Phi}^{(0)} \right)^3 + O \left( \delta\hat{\Phi}^{(0)} \right)^4 \right] \delta\hat{\Phi}_n^{(0)} \quad (\text{C5})$$

We stress that the terms  $q_{0,n}$ ,  $q_{1,n}$ ,  $q_{2,n}$  and  $q_{3,n}$  are coefficients of a Taylor expansion and result to be functions of the external bias conditions (i.e., of the constant flux difference  $\Delta\Phi_{DC}$ ). It's worth noting here how the lowest perturbative order approach adopted in equation (C4) takes into account interactions of modes at the first order, that means a single multimodes interaction. While the power expansion truncation up to the third order in equation (C5) limits our model to the interaction of a single mode ( $\delta\hat{\Phi}_n^{(0)}$ ) with up to three modes. For a quantitative comparison of the power expansion approach (C5) respect to the bare nonlinearity (C4) see Figure 7.

#### Appendix D: Coupling Coefficients

Defined  $p_1 = \cos(\Delta\Phi_{DC}/\varphi_0)$  and  $p_2 = \sin(\Delta\Phi_{DC}/\varphi_0)$ :

$$\chi_0 = \frac{N}{\hbar} \left[ I_c \varphi_0 \left( 1 - \cos \left( \frac{\Delta\Phi_{DC}}{\varphi_0} \right) \right) + \frac{\Delta\Phi_{DC}^2}{2L_g} \right] \quad (\text{D1})$$

$$\chi_1^{(n)} = \frac{\omega_n}{2} \left( 1 + 2L_g \Lambda_n \left[ \left( I_c p_2 + \frac{\Delta\Phi_{DC}}{L_g} \right) q_{1,n} + \left( \frac{I_c p_1}{\varphi_0} + \frac{1}{L_g} + C_J \Delta\omega_n^2 \right) \frac{q_{0,n}^2}{2} \right] \right) \quad (\text{D2})$$

$$\begin{aligned} \chi_3^{(n,l,m)} = & \sqrt{\frac{\hbar L_g^3}{8N}} \sqrt{\omega_n \Lambda_n \omega_l \Lambda_l \omega_m \Lambda_m} \left[ \left( I_c p_2 + \frac{\Delta\Phi_{DC}}{L_g} \right) q_{2,n} + \left( \frac{I_c p_1}{\varphi_0} + \frac{1}{L_g} \right) q_{0,n} q_{1,l} + \right. \\ & \left. - \frac{I_c p_2}{6\varphi_0^2} q_{0,n} q_{0,l} q_{0,m} + \frac{C_J}{2} [q_{0,n} q_{1,l} \Delta\omega_n \Delta\omega_{m,l} + q_{1,n} q_{0,l} \Delta\omega_l \Delta\omega_{n,m}] \right] \end{aligned} \quad (\text{D3})$$

$$\begin{aligned} \chi_4^{(n,l,m,s)} = & \frac{\hbar L_g^2}{4N} \sqrt{\omega_n \Lambda_n \omega_l \Lambda_l \omega_m \Lambda_m \omega_s \Lambda_s} \left[ \left( I_c p_2 + \frac{\Delta \Phi_{DC}}{L_g} \right) q_{3,n} + \frac{1}{2} \left( \frac{I_c p_1}{\varphi_0} + \frac{1}{L_g} \right) (2q_{0,n} q_{2,l} + q_{1,n} q_{1,l}) + \right. \\ & - \frac{I_c p_2}{2\varphi_0^2} q_{1,n} q_{0,l} q_{0,m} - \frac{I_c p_1}{24\varphi_0^3} q_{0,n} q_{0,l} q_{0,m} q_{0,s} + \\ & \left. + \frac{C_J}{2} [q_{1,n} q_{1,l} (\Delta \omega_m \Delta \omega_{s,l} + \Delta \omega_n \Delta \omega_{m,l}) + q_{2,n} q_{0,l} \Delta \omega_l \Delta \omega_{2m,n} + q_{0,n} q_{2,l} \Delta \omega_n \Delta \omega_{2m,l}] \right] \end{aligned} \quad (D4)$$

### Appendix E: Time evolution of the ladder operators: coupled mode equations

Starting from equation (11) and (12) it is possible to work out the dynamics of the system in 3WM and 4WM regime.

In 3WM regime, hence using (11) to compute the Heisenberg equation it is obtained

$$\frac{d\hat{a}_p}{dt} = \frac{i}{\hbar} [\hat{H}_{3WM}^{\{p,s,i\}}, \hat{a}_p] = -i [\chi_1^p \hat{A}_p + \chi_3^{\{p,s,i\}} \hat{a}_s \hat{a}_i] \quad (E1)$$

$$\frac{d\hat{a}_s}{dt} = \frac{i}{\hbar} [\hat{H}_{3WM}^{\{p,s,i\}}, \hat{a}_s] = -i [\chi_1^s \hat{a}_s + \chi_3^{\{p,s,i\}} \hat{A}_p \hat{a}_i^\dagger] \quad (E2)$$

$$\frac{d\hat{a}_i}{dt} = \frac{i}{\hbar} [\hat{H}_{3WM}^{\{p,s,i\}}, \hat{a}_i] = -i [\chi_1^i \hat{a}_i + \chi_3^{\{p,s,i\}} \hat{A}_p \hat{a}_s^\dagger] \quad (E3)$$

While in 4WM regime, through (12)

$$\begin{aligned} \frac{d\hat{a}_p}{dt} = & \frac{i}{\hbar} [\hat{H}_{4WM}^{\{p,s,j\}}, \hat{a}_p] \\ = & -i \left[ (\xi_p + \xi_{pp} + 2\xi_{pp} \hat{A}_p^\dagger \hat{A}_p + \right. \\ & \left. + \xi_{ps} \hat{a}_s^\dagger \hat{A}_p + \xi_{pj} \hat{a}_j^\dagger \hat{a}_j) \hat{A}_p + 2\chi_4^{\{p,p,s,i\}} \hat{A}_p^\dagger \hat{a}_s \hat{a}_j \right] \end{aligned} \quad (E4)$$

$$\begin{aligned} \frac{d\hat{a}_s}{dt} = & \frac{i}{\hbar} [\hat{H}_{4WM}^{\{p,s,i\}}, \hat{a}_s] \\ = & -i \left[ (\xi_s + \xi_{ss} + 2\xi_{ss} \hat{a}_s^\dagger \hat{a}_s + \xi_{ps} \hat{A}_p^\dagger \hat{A}_p + \right. \\ & \left. + \xi_{sj} \hat{a}_j^\dagger \hat{a}_j) \hat{a}_s + \chi_4^{\{p,p,s,i\}} \hat{A}_p \hat{A}_p \hat{a}_s^\dagger \right] \end{aligned} \quad (E5)$$

$$\begin{aligned} \frac{d\hat{a}_i}{dt} = & \frac{i}{\hbar} [\hat{H}_{4WM}^{\{p,s,i\}}, \hat{a}_i] \\ = & -i \left[ (\xi_j + \xi_{jj} + 2\xi_{jj} \hat{a}_i^\dagger \hat{a}_j + \xi_{pj} \hat{A}_p^\dagger \hat{A}_p + \right. \\ & \left. + \xi_{sj} \hat{a}_s^\dagger \hat{a}_s) \hat{a}_i + \chi_4^{\{p,p,s,j\}} \hat{A}_p \hat{A}_p \hat{a}_s^\dagger \right] \end{aligned} \quad (E6)$$

The systems composed by equations (E1), (E2), (E3) and by equations (E4), (E5), (E6) are known as Quantum Langevin Equations (also Coupled Mode Equations in the classical regime), and their solutions determine the time evolution of the modes interacting into the TWJPA. The undepleted pump approximation describes a regime where the signal and idler modes can be considered small compared to the pump mode. This approximation allows to solve analytically the system of coupled differential equations by substituting the ladder operator of the pump mode with its classical counterpart, having defined

$$\sqrt{\frac{2\hbar\omega_p}{C_g N}} \hat{a}_p \mapsto A_p \quad (E7)$$

as the classical voltage amplitude of Eq. (4). In the 4M case, equation (E7) can be substituted into (E4)

$$\begin{aligned} \sqrt{\frac{C_g N}{2\hbar\omega_p}} \frac{dA_p}{dt} = & -i \left[ (\xi_p + \xi_{pp}) \sqrt{\frac{C_g N}{2\hbar\omega_p}} A_p + \right. \\ & + 2 \left( \frac{C_g N}{2\hbar\omega_p} \right)^{\frac{3}{2}} |A_p|^2 \xi_{pp} A_p + \xi_{ps} \sqrt{\frac{C_g N}{2\hbar\omega_p}} A_p \hat{a}_s^\dagger \hat{a}_s + \\ & + \xi_{pj} \sqrt{\frac{C_g N}{2\hbar\omega_p}} \hat{a}_j^\dagger \hat{a}_j A_p + 2\chi_4^{\{p,p,s,j\}} \sqrt{\frac{C_g N}{2\hbar\omega_p}} A_p^* \hat{a}_s \hat{a}_j \left. \right] \\ \frac{dA_p}{dt} = & -i \left[ (\xi_p + \xi_{pp}) A_p + 2 \frac{C_g N}{2\hbar\omega_p} |A_p|^2 \xi_{pp} A_p + \right. \\ & + \xi_{ps} A_p \hat{a}_s^\dagger \hat{a}_s + \xi_{pj} \hat{a}_j^\dagger \hat{a}_j A_p + 2\chi_4^{\{p,p,s,j\}} A_p^* \hat{a}_s \hat{a}_j \left. \right] \end{aligned} \quad (E8)$$

Keeping the leading terms in (E8) we get

$$\begin{aligned} \frac{dA_p}{dt} \approx & -i \left[ (\xi_p + \xi_{pp}) A_p + 2 \frac{C_g N}{2\hbar\omega_p} |A_p|^2 \xi_{pp} A_p \right] \\ = & -i \left( (\xi_p + \xi_{pp}) + 2 \frac{C_g N}{2\hbar\omega_p} |A_p|^2 \xi_{pp} \right) A_p \\ = & -i \Psi_p A_p \end{aligned} \quad (E9)$$

and by solving this latter, one can derive

$$A_p(t) = |A_{p,0}|e^{-i\Psi_p t} \quad (\text{E10})$$

with

$$\Psi_p = \xi_p + \xi_{pp} + 2\xi_{pp} \frac{C_g N}{2\hbar\omega_p} |A_p|^2 \quad (\text{E11})$$

$|A_{p,0}|$  is the voltage amplitude at  $t = 0$ , the time in which the mode enters in the non-linear medium. For sake of simplicity we have assumed the initial phase of  $A_p$  equal to zero. Similarly, the time evolution for the signal and idler annihilation operators can be written as

$$\begin{aligned} \frac{d\hat{a}_s}{dt} &= -i \left[ \left( \xi_s + \xi_{ss} + 2\xi_{ss} \hat{a}_s^\dagger \hat{a}_s + \xi_{ps} \left( \frac{C_g N}{2\hbar\omega_p} \right) |A_p|^2 + \right. \right. \\ &\quad \left. \left. + \xi_{si} \hat{a}_j^\dagger \hat{a}_j \right) \hat{a}_s + \chi_4^{\{p,p,s,j\}} \left( \frac{C_g N}{2\hbar\omega_p} \right) A_p^2 \hat{a}_j^\dagger \right] \\ &\approx -i \left[ \left( \xi_s + \xi_{ps} \left( \frac{C_g N}{2\hbar\omega_p} \right) |A_p|^2 \right) \hat{a}_s + \right. \\ &\quad \left. + \chi_4^{\{p,p,s,j\}} \left( \frac{C_g N}{2\hbar\omega_p} \right) A_p^2 \hat{a}_j^\dagger \right] \\ &= -i \left[ \Psi_s \hat{a}_s + \chi_4^{\{p,p,s,j\}} \left( \frac{C_g N}{2\hbar\omega_p} \right) A_p^2 \hat{a}_j^\dagger \right] \quad (\text{E12}) \end{aligned}$$

with

$$\Psi_s = \xi_s + \xi_{ps} \left( \frac{C_g N}{2\hbar\omega_p} \right) |A_p|^2 \quad (\text{E13})$$

In the co-rotating frame

$$\begin{aligned} \frac{d\hat{a}_s}{dt} &= -i \chi_4^{\{p,p,s,j\}} \left( \frac{C_g N}{2\hbar\omega_p} \right) A_p^2 (\hat{a}_j^{CR})^\dagger e^{i(\Psi_s + \Psi_j)t} \\ &= -i \chi_4 |A_{p,0}|^2 (\hat{a}_j^{CR})^\dagger e^{-i(2\Psi_p - \Psi_s - \Psi_j)t} \\ &= -i \chi_4 |A_{p,0}|^2 (\hat{a}_j^{CR})^\dagger e^{-i\Psi_4 t} \quad (\text{E14}) \end{aligned}$$

where equation (E10) has been exploited, having

$$\Psi_4 = 2\Psi_p - \Psi_s - \Psi_j \quad (\text{E15})$$

and introducing

$$\chi_4 = \chi_4^{\{p,p,s,j\}} \frac{C_g N}{2\hbar\omega_p} \quad (\text{E16})$$

The 3WM system can be solved through the same procedure starting from equation (E1)

$$\begin{aligned} \frac{d\hat{a}_p}{dt} &= \frac{i}{\hbar} \left[ \hat{H}_{3\text{WM}}^{\{p,s,i\}}, \hat{a}_p \right] \\ \frac{dA_p}{dt} &= -i \left[ \chi_1^p \hat{A}_p + \chi_3^{\{p,s,i\}} \hat{a}_s \hat{a}_i \right] \approx -i \chi_1^p A_p \quad (\text{E17}) \end{aligned}$$

whose solution is

$$A_p(t) = |A_{p,0}|e^{-i\chi_1^p t} \quad (\text{E18})$$

equation (E2) becomes

$$\frac{d\hat{a}_s}{dt} = -i \left[ \chi_1^s \hat{a}_s + \chi_3^{\{p,s,i\}} \sqrt{\frac{C_g N}{2\hbar\omega_p}} |A_{p,0}| \hat{a}_s^\dagger e^{-i\chi_1^p t} \right] \quad (\text{E19})$$

in the co-rotating frame

$$\begin{aligned} \frac{d\hat{a}_s}{dt} &= -i \chi_3^{\{p,s,i\}} \sqrt{\frac{C_g N}{2\hbar\omega_p}} |A_{p,0}| \hat{a}_s^\dagger e^{-i(\chi_1^p - \chi_1^s - \chi_1^i)t} \\ &= -i \chi_3 |A_{p,0}| \hat{a}_s^\dagger e^{-i\Psi_3 t} \quad (\text{E20}) \end{aligned}$$

$$\begin{aligned} \frac{d\hat{a}_i}{dt} &= -i \chi_3^{\{p,s,i\}} \sqrt{\frac{C_g N}{2\hbar\omega_p}} |A_{p,0}| \hat{a}_i^\dagger e^{-i(\chi_1^p - \chi_1^s - \chi_1^i)t} \\ &= -i \chi_3 |A_{p,0}| \hat{a}_i^\dagger e^{-i\Psi_3 t} \quad (\text{E21}) \end{aligned}$$

with

$$\Psi_3 = \chi_1^p - \chi_1^s - \chi_1^i \quad (\text{E22})$$

and

$$\chi_3 = \sqrt{\frac{C_g N}{2\hbar\omega_p}} \chi_3^{\{p,s,i\}} \quad (\text{E23})$$

## Appendix F: Squeezing

The correlation of the signal and idler photons results in a so-called squeezed output field of a TWJPA. One can define the thermal photon number as

$$N(\omega) = \int_0^\infty d\omega' (\langle \hat{a}_\omega^\dagger \hat{a}_{\omega'} \rangle - \langle \hat{a}_\omega^\dagger \rangle \langle \hat{a}_{\omega'} \rangle) \quad (\text{F1})$$

and the squeezing parameter as

$$M(\omega) = \int_0^\infty d\omega' (\langle \hat{a}_\omega \hat{a}_{\omega'} \rangle - \langle \hat{a}_\omega \rangle \langle \hat{a}_{\omega'} \rangle) \quad (\text{F2})$$

From the definitions (25) and (26) one can compute the relation between the squeezing spectrum ( $S$ ), the thermal photon number and the squeezing parameter

$$\begin{aligned} S(\omega) &= \int_0^\infty d\omega' \langle \Delta \hat{Y}^\theta(\omega) \Delta \hat{Y}^\theta(\omega') \rangle \\ &= 1 + 2N(\omega) - 2|M(\omega)| \quad (\text{F3}) \end{aligned}$$

For a vacuum input state, the number of thermal photons can be easily calculated through equations (16)

$$N(\omega) = |v(\omega, t)|^2 \quad (\text{F4})$$

Again using (16), the squeezing parameter for a vacuum input state can be written as

$$\begin{aligned} M(\omega) &= \int_0^\infty d\Omega (\langle \hat{a}_\omega \hat{a}_\Omega \rangle - \langle \hat{a}_\omega \rangle \langle \hat{a}_\Omega \rangle) \\ &= \int_0^\infty d\Omega \langle \hat{a}_\omega \hat{a}_\Omega \rangle \\ &= \int_0^\infty d\Omega \langle \text{vac} | \left( u(\omega, t) \hat{a}_{\omega,0} + iv(\omega, t) \hat{a}_{\omega'}^\dagger \right) \\ &\quad \cdot \left( u(\Omega, t) \hat{a}_{\Omega,0} + iv(\Omega, t) \hat{a}_{\Omega'}^\dagger \right) | \text{vac} \rangle e^{-i\Psi t} \\ &= iu(\omega, t) e^{-i\Psi t} \int_0^\infty d\Omega v(\Omega, t) \langle \text{vac} | \hat{a}_{\omega,0} \left( \hat{a}_{\Omega',0} \right)^\dagger | \text{vac} \rangle \\ &= iu(\omega, t) v(\omega', t) e^{-i\Psi t} \\ &= iu(\omega, t) v(\omega, t) e^{-i\Psi t} \\ &= \left( \frac{\Psi \chi_3 |A_{p,0}|}{2g^2} \sinh^2(gt) - i \frac{\chi_3 |A_{p,0}|}{g} \sinh(gt) \cosh(gt) \right) e^{-i\Psi t} \\ &= |u(\omega, t) v(\omega, t)| e^{-i \left( \arctan \left( \frac{2g}{\Psi} \coth(gt) \right) + \Psi t \right)} = \\ &= |M(\omega)| e^{i\theta} \end{aligned} \quad (\text{F5})$$

Where we exploited  $v(\omega') = v(\omega)$  and identified the squeezing angle as

$$\theta = - \left( \arctan \left( \frac{2g}{\Psi} \coth gt \right) + \Psi t \right) \quad (\text{F6})$$

Hence one can easily find the relation between  $M(\omega)$  and  $N(\omega)$  as

$$\begin{aligned} |M(\omega)|^2 &= |u(\omega, t) v(\omega, t)|^2 \\ &= |u(\omega, t)|^2 |v(\omega, t)|^2 \\ &= (|v(\omega, t)|^2 + 1) |v(\omega, t)|^2 \\ &= N(\omega) [N(\omega) + 1] \end{aligned} \quad (\text{F7})$$

that is the maximum allowed by the Heisenberg uncertainty principle and implies that the amplification is quantum limited [27].

---

[1] R. H. Hadfield, "Single-photon detectors for optical quantum information applications," *Nature Photonics*, vol. 3, no. 12, pp. 696–705, 2009.

[2] C. M. Natarajan, M. G. Tanner, and R. H. Hadfield, "Superconducting nanowire single-photon detectors: physics and applications," *Superconductor Science and Technology*, vol. 25, p. 063001, apr 2012.

[3] J. Ullom, W. Doriese, D. Fischer, J. Fowler, G. Hilton, C. Jaye, C. Reintsema, D. Swetz, and D. Schmidt, "Transition-edge sensor microcalorimeters for x-ray beamline science," *Synchrotron Radiation News*, vol. 27, no. 4, pp. 24–27, 2014.

[4] D. Fukuda, G. Fujii, T. Numata, K. Amemiya, A. Yoshizawa, H. Tsuchida, H. Fujino, H. Ishii, T. Itatani, S. Inoue, and T. Zama, "Titanium-based transition-edge photon number resolving detector with 98% detection efficiency with index-matched small-gap fiber coupling," *Optics Express*, vol. 19, pp. 870–875, Jan 2011.

[5] A. J. Miller, S. W. Nam, J. M. Martinis, and A. V. Sergienko, "Demonstration of a low-noise near-infrared photon counter with multiphoton discrimination," *Applied Physics Letters*, vol. 83, no. 4, pp. 791–793, 2003.

[6] A. E. Lita, A. J. Miller, and S. W. Nam, "Counting near-infrared single-photons with 95% efficiency," *Optics Express*, vol. 16, pp. 3032–3040, Mar 2008.

[7] R. Yang and H. Deng, "Fabrication of the impedance-matched Josephson parametric amplifier and the study of the gain profile," *IEEE Transactions on Applied Superconductivity*, pp. 1–1, 2020.

[8] M. Malnou, D. A. Palken, L. R. Vale, G. C. Hilton, and K. W. Lehnert, "Optimal operation of a Josephson parametric amplifier for vacuum squeezing," *Physical Review Applied*, vol. 9, p. 044023, Apr 2018.

[9] M. A. Castellanos-Beltran, K. D. Irwin, L. R. Vale, G. C. Hilton, and K. W. Lehnert, "Bandwidth and dynamic range of a widely tunable Josephson parametric amplifier," *IEEE Transactions on Applied Superconductivity*, vol. 19, pp. 944–947, June 2009.

[10] C. Eichler and A. Wallraff, "Controlling the dynamic range of a Josephson parametric amplifier," *EPJ Quantum Technology*, vol. 1, no. 1, p. 2, 2014.

[11] T. C. White, J. Y. Mutus, I.-C. Hoi, R. Barends, B. Campbell, Y. Chen, Z. Chen, B. Chiaro, A. Dunsworth, E. Jeffrey, J. Kelly, A. Megrant, C. Neill, P. J. J. O'Malley, P. Roushan, D. Sank, A. Vainsencher, J. Wenner, S. Chaudhuri, J. Gao, and J. M. Martinis, "Traveling wave parametric amplifier with Josephson junctions using minimal resonator phase matching," *Applied Physics Letters*, vol. 106, no. 24, p. 242601, 2015.

[12] C. Macklin, K. O'Brien, D. Hover, M. E. Schwartz, V. Bolkhovsky, X. Zhang, W. D. Oliver, and I. Siddiqi, "A near-quantum-limited Josephson traveling-

wave parametric amplifier,” *Science*, vol. 350, no. 6258, pp. 307–310, 2015.

[13] N. Zobrist, B. H. Eom, P. Day, B. A. Mazin, S. R. Meeker, B. Bumble, H. G. LeDuc, G. Coiffard, P. Szypryt, N. Fruitwala, I. Lipartito, and C. Bockstiegel, “Wide-band parametric amplifier readout and resolution of optical microwave kinetic inductance detectors,” *Applied Physics Letters*, vol. 115, no. 4, p. 042601, 2019.

[14] S. Chaudhuri, D. Li, K. D. Irwin, C. Bockstiegel, J. Hubmayr, J. N. Ullom, M. R. Vissers, and J. Gao, “Broadband parametric amplifiers based on nonlinear kinetic inductance artificial transmission lines,” *Applied Physics Letters*, vol. 110, no. 15, p. 152601, 2017.

[15] M. R. Vissers, R. P. Erickson, H.-S. Ku, L. Vale, X. Wu, G. C. Hilton, and D. P. Pappas, “Low-noise kinetic inductance traveling-wave amplifier using three-wave mixing,” *Applied Physics Letters*, vol. 108, no. 1, p. 012601, 2016.

[16] A. B. Zorin, “Josephson traveling-wave parametric amplifier with three-wave mixing,” *Physical Review Applied*, vol. 6, p. 034006, Sep 2016.

[17] A. B. Zorin, M. Khabipov, J. Dietel, and R. Dolata, “Traveling-wave parametric amplifier based on three-wave mixing in a Josephson metamaterial,” in *2017 16th International Superconductive Electronics Conference (ISEC)*, pp. 1–3, June 2017.

[18] T. M. Buehler, D. J. Reilly, R. P. Starrett, A. D. Green-tree, A. R. Hamilton, A. S. Dzurak, and R. G. Clark, “Single-shot readout with the radio-frequency single-electron transistor in the presence of charge noise,” *Applied Physics Letters*, vol. 86, no. 14, p. 143117, 2005.

[19] A. Aassime, G. Johansson, G. Wendum, R. J. Schoelkopf, and P. Delsing, “Radio-frequency single-electron transistor as readout device for qubits: Charge sensitivity and backaction,” *Physical Review Letter*, vol. 86, pp. 3376–3379, Apr 2001.

[20] S. W. Henderson, Z. Ahmed, J. Austermann, D. Becker, D. A. Bennett, D. Brown, S. Chaudhuri, H.-M. S. Cho, J. M. D’Ewart, B. Dober, S. M. Duff, J. E. Dusatko, S. Fatigoni, J. C. Frisch, J. D. Gard, M. Halpern, G. C. Hilton, J. Hubmayr, K. D. Irwin, E. D. Karpel, S. S. Kernasovskiy, S. E. Kuenstner, C.-L. Kuo, D. Li, J. A. B. Mates, C. D. Reintsema, S. R. Smith, J. Ullom, L. R. Vale, D. D. V. Winkle, M. Vissers, and C. Yu, “Highly-multiplexed microwave SQUID readout using the SLAC Microresonator Radio Frequency (SMuRF) electronics for future CMB and sub-millimeter surveys,” in *Millimeter, Submillimeter, and Far-Infrared Detectors and Instrumentation for Astronomy IX* (J. Zmuidzinas and J.-R. Gao, eds.), vol. 10708, pp. 170 – 185, International Society for Optics and Photonics, SPIE, 2018.

[21] X. Guo, C.-l. Zou, C. Schuck, H. Jung, R. Cheng, and H. X. Tang, “Parametric down-conversion photon-pair source on a nanophotonic chip,” *Light: Science & Applications*, vol. 6, no. 5, pp. e16249–e16249, 2017.

[22] T. H. A. van der Reep, “Mesoscopic hamiltonian for josephson traveling-wave parametric amplifiers,” *Physical Review A*, vol. 99, p. 063838, Jun 2019.

[23] A. B. Arne L. Grimsmo, “Squeezing and quantum state engineering with Josephson travelling wave amplifiers,” *npj Quantum Information*, 2017.

[24] R. Loudon, *The Quantum Theory of Light, third edition*. Oxford Science Publication, 2000.

[25] U. Vool and M. Devoret, “Introduction to quantum electromagnetic circuits,” *International Journal of Circuit Theory and Applications*, vol. 45, no. 7, pp. 897–934, 2017.

[26] R. Gambini, “Parametric amplification with a trilinear Hamiltonian,” *Physical Review A*, vol. 15, no. 3, pp. 1157–1168, 1977.

[27] E. Jeffrey, D. Sank, J. Y. Mutus, T. C. White, J. Kelly, R. Barends, Y. Chen, Z. Chen, B. Chiaro, A. Dunsworth, A. Megrant, P. J. J. O’Malley, C. Neill, P. Roushan, A. Vainsencher, J. Wenner, A. N. Cleland, and J. M. Martinis, “Fast accurate state measurement with superconducting qubits,” *Physical Review Letter*, vol. 112, p. 190504, May 2014.